Original Research Paper

JIC *Journal of Industrial Catalysis Vol. 1, No. 1, 2023, 9-1۳.*

Evaluation of new integrated photo-catalyst adsorbent for removal of haloacetonitriles from water

Ehsan Ghorban Nezhad[1], Behrooz Mahmoodzadeh Vaziri[1]

[1] *Department of Chemical engineering, Quchan branch, Islamic Azad University, Quchan, Iran*

* vaziri@iauq.ac.ir, behrouz.vaziri@gmail.com

Received 8 March 2023; accepted 16 April 2023

Abstract

In this study, a new integrated photo-catalyst adsorbent is prepared to degrade the harmful organic compounds of water in the presence of light irradiation. A citric acid assisted sol-gel method was employed to perovskite $MoTiO_3$/GO nanocomposites preparation. The characteristics of the samples were performed by SEM, BET, FTIR and XRD analysis. Results showed that the synthesized $MoTiO_3$ nanoparticles with average size of 26 nm were successfully deposited onto the graphene oxide (GO) adsorbent. Increasing the content of GO up to 1.5 wt. % in nanocomposite has an increasing effect on specific surface area. MoTiO3/GO photocatalytic activity was investigated by the haloacetonitriles (HANs) decomposition under UV irradiation. The $MoTiO_3$/ (GO, 1.5wt. %) nanocomposite displayed significant HANs removal capability up to 98.24% and excellent photocatalytic activity after 120 minutes of UV irradiation. Therefore, it can be said that the $MoTiO_3$/GO is a potential photo-catalyst for effective wastewater treatment of disinfection by-products (DBPs) and future industrial applications.

Keywords: *Graphene oxide, Haloacetonitrile, MoTiO3 nanocomposite, Photo-catalyst adsorbent*

1. Introduction

A safe supply of drinking water is vital to our health and well-being. Untreated water sources can contain harmful microorganisms that can cause serious problems or, in some cases, death [1]. Chlorination of drinking water is a proven method with an excellent safety record [2]. Many people around the world receive quality-disinfected drinking water from public water supplies, but chemical disinfection has created health problems. Chlorine is present in disinfected water in the form of hypochlorite and hypochlorous acid, which reacts with organic substances such as humic acid and fulvic acid, and disinfection byproducts include haloacetic acid (HAAs), trihalomethane (THM), chlorophenols, and haloacetonitriles (HANs) creates [3]. HANs are nitrogenous disinfection by-products (DBPs) that formed by the reaction between chlorine, chloramine or bromine disinfectants and natural organic matter present in drinking water supplies [4]. There are many different types of methods such as membrane filtration [5], adsorption [6-8], ozonation [9], photo-catalyst [10], etc. have been used to eliminate the DBPs from water effectively.

Photo-catalysts have the ability to destroy organic and inorganic pollutants using visible light, so it has the best potential to replace conventional wastewater treatment technology. Various compounds have been used as photo-catalysts for photo-degradation of many pollutants from water [11]. However, using these materials has its own problems. The main drawback of photo-catalytic nanoparticles is that they agglomerate when used in slurry form, which greatly reduces photo-catalytic performance [12-14]. The polar and non-porous surface of the photo-catalyst also reduces adsorption of impurities to its surface, thereby reducing the rate of photo-degradation. The photo-catalyst immobilization on the adsorbents is one of method that used to treat these problems.

An integrated photo-catalyst adsorbent can be degraded the harmful organic compounds in the presence of UV/visible light irradiation [15]. This combination preserves the properties of both individual components and overcomes to the problems such as fast recombination of photo-generated electrons and low absorptivity [16]. There had been many support materials that exhibit high specific surface area and dispersing ability which enhance excellent performance. Graphene oxide (GO) is one of the materials that is widely used in wastewater treatment due to its unique properties such as large surface area, mechanical stability, tunable electrical and optical properties [17].

In this work, the novel perovskite $MoTiO_3$/GO nanocomposite has been prepared and introduced. The characterizations of $MoTiO_3$/GO nanocomposite were done by scanning electron microscopy (SEM), fourier transform infrared spectra (FTIR), Brunauer-Emmett-Teller (BET) and X-ray diffraction (XRD) analysis. Finally, adsorption and photocatalytic activity evaluation of nanocomposite were examined on haloacetonitriles.

2. Experimental

$(NH_4)_6Mo_7O_{24}•_4H_2O$, Ti $(NO_3)_4$ and citric acid were supplied from Sigma-Aldrich (USA). GO was purchased from Merck (Germany). A mixture of haloacetonitriles including chloroacetonitrile (C2H2ClN), dichloroacetonitrile (C2HCl2N), trichloroacetonitrile (C2Cl3N), bromo-acetonitrile (C2H2BrN), and dibromoacetonitrile (C2HBr2N) were supplied from Alfa Aesar (Ward 116 Hill, MA).

2.1 Graphene oxide pre-treatment

The following procedure was done to graphene oxide pretreatment:

At the beginning, 3 grams of graphene oxide were refluxed in 150 ml of 2 M potassium hydroxide solution containing 1% by weight of sodium dodecyl sulfate at 120°C for 2 hours. Then the resulting mixture was cooled at room temperature, washed with DI water and filtered through a filter membrane with a pore diameter of 0.2 μm. Next, the sample was refluxed in concentrated nitric acid (65wt. %) for 24 hours with continuous stirring. The final product was washed with DI water and dried at room temperature.

2.2 MoTiO3-GO nanocomposite preparation

Sol-gel citrate method was used to prepare MoTiO3/GO nanocomposite. At first, equimolar of titanium nitrate (Ti (NO3)4) and ammonium heptamolybdate tetra hydrate ((NH4)6Mo7O24•4H2O) precursors were mixed by DI water. Then sol-gel agent (citric acid) was added in to the above mixture and the pH was adjusted to 6 by (NH4)2CO3 (1M). After stirring and sonicating the solution for 10 minutes, 5 grams of GO (at different concentrations of 0.5, 1, 1.5 and 2wt.%) were added to the resulting mixture and the mixture suspension was stirred and the temperature was set to 60°C and evaporated to obtain the sol-gel. The resulting gel was formed by the decomposition of nitrate ions due to the release of NOx gas. Then it was dried in a vacuum oven at 100°C for 3 hours. Then, the precursor is calcined at 1000°C for 5 h with a heating rate of 5 °C/min, and the final product was marked as MoTiO3/GO.

2.3. Characterization

The morphology of samples was characterized using SEM (KYKY-EM3200) with an accelerating voltage of 26 kV. The structural study of the samples was evaluated by BET (Micrometrics, ASAP 2020 analyzer). XRD measurements of cast PEDOU membranes were conducted on a DJ-10 Mini Desktop X-ray with Cu Kα radiation (wavelength: 1.5 Å) at 45 kV and 20 mA. FTIR was done by a Nicolet Nexus 670 FTIR spectrophotometer to identify the functional groups of integrated photo-catalyst adsorbent.

2.4 Adsorption and photo-catalytic study

The degradation experiment of HANs was carried out in a Xenon Lamp Photo-chemical Reactor (BL-GHX-I model) equipped with a 500W medium pressure Xenon lamp as the illumination source (wave length λ> 400nm, irradiation intensity 122.5 mW/cm2). In a typical adsorption and photo-catalytic measurements, 2 mg of integrated photo-catalyst adsorbent material was added into 150 mL HANs solution and sonicated for 20 min. To achieve the enrichment of adsorption-desorption equilibrium among the $MoTiO_3$-GO and HANs solution, the mixture was stirred in a dark continuously at least in 60 min at ambient temperature and pressure. Then, a sample was taken from the supernatant solution and the equilibrium concentrations of HANs was determined by a gas chromatography–mass spectrometry (GC–MS) (GCMS-QP2010 SE, Shimadzu, Japan). The adsorption performance for HANs removal was calculated using Eq. (1) [18]:

$$\text{HANs Removal (\%)} = (C_0-C_f)/C_0 \times 100 \quad (1)$$

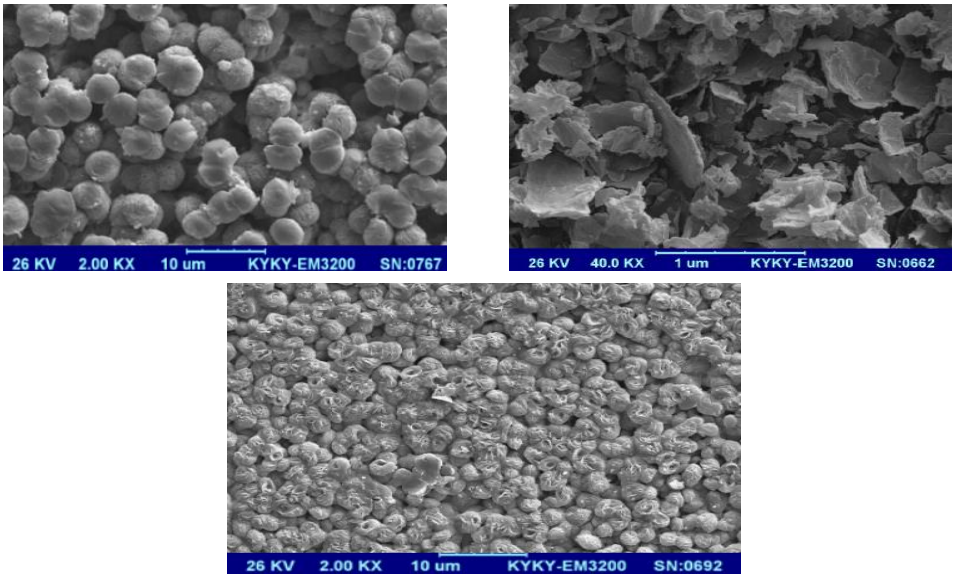

Fig. 1. SEM images of (a) $MoTiO_3$, (b) GO, and (c) $MoTiO_3$/ (GO 1.5 wt. %).

Where Co (mg/L) and Cf (mg/L) are the initial and the final HANs concentrations respectively. Then for evaluation of photo-catalytic degradation, the mixed suspension was transferred to the photochemical reactor under visible light irradiation at ambient temperature for 1 hour with a mixing rate of 500 rpm. During the photo-catalytic reaction, a small amount of the suspension was sampled at a certain time interval (15 min). The HANs degradation procedure was monitored by measuring supernatant concentration using the GC–MS.

3. Results and discussion

SEM analysis is used to evaluate the morphological characteristics of prepared composite nanomaterials. Fig.1 (a-c) shows spongy distinct particles of $MoTiO_3$, the folded layer surface of GO, and spherical particles of $MOTiO_3$/GO, respectively. Fig. 1 (c) indicates a porous structure with large voids, which is attributed to the gas release during the gel preparation.

The BET method was used to evaluation of samples surface area. As can be seen in Fig. 2 (a), the IV type with a H3 hysteresis loops observe for MoTiO3/ (GO 1.5 wt. %) samples that indicates the mesoporous structure. The hysteresis loop is not existence for MoTiO3 which shows its small surface area (Fig. 2 (b)).

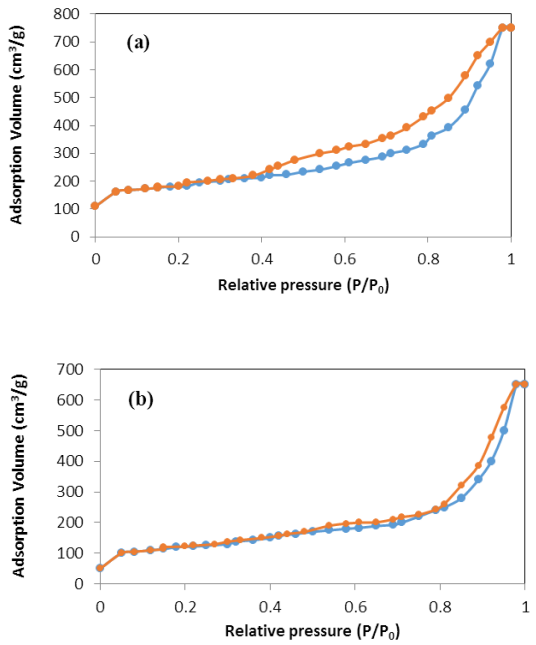

Fig. 2. (a) Nitrogen adsorption-desorption isotherms of $MoTiO_3$/GO nanocomposite and (b) $MoTiO_3$.

The area of nanocomposite samples is shown in Table 1. By increasing GO content up to 1.5 wt.%, the total surface area of integrated photo-catalyst adsorbent increased and then it began to decline when GO content reached to 2 wt.%. The sample without GO observed small surface area. It might be due to particle's coalesce and relatively large crystallite size. In $MoTiO_3$/GO samples with GO content up to 1.5 wt. %, the uniform distribution of $MoTiO_3$ on GO causes a higher specific surface area than $MoTiO_3$. At higher amounts of GO (> 1.5 wt. %), GO agglomeration occurs, which is leading to decline the specific surface.

Table 1. Total surface area of prepared samples measured by BET method

samples	Total surface area (m^2g^{-1})
$MoTiO_3$/GO (0 wt.% $MoTiO_3$)	40.3
$MoTiO_3$/GO (0 wt.% GO)	8.9
$MoTiO_3$/GO (0.5 wt.% GO)	18.2
$MoTiO_3$/GO (1 wt.% GO)	25.2
$MoTiO_3$/GO (1.5 wt.% GO)	36.4
$MoTiO_3$/GO (2 wt.% GO)	29.1

Fig. 3 shows the FTIR spectrum of GO, $MoTiO_3$ and $MoTiO_3$/GO. In the FTIR spectra of GO, the C=O stretching vibration band is evident at 1734 cm^{-1}. Also C-O stretching vibration at 1038 cm^{-1}, O-H stretching vibration at 3322 cm^{-1} and vibration of unoxidized graphitic domains at 1622 cm^{-1} were observed.

In Fig. 3, the peaks at 3382 and 1621 cm^{-1} in the FTIR spectrum of $MoTiO_3$ were attributed to the characteristic absorptions of hydroxyl vibration. This hydroxyl group was derived from the adsorption water on the surface of the sample. Also, the Mo-Ti-O bond in the $MoTiO_3$ exhibit the adsorption peak at 552 cm^{-1}. In FTIR spectra of $MoTiO_3$/GO adsorbent, some of vibration bands had shifted to lower frequency due to the existence of an intermolecular interaction between the $MoTiO_3$ and GO.

The average pore size distribution in Fig. 4 shows the average pore size of GO is about 3-4 nm. Also, MoTiO3 showed a wide pore size distribution of about 26 nm. It is noteworthy that the pore size distribution of MoTiO3/GO is not significantly different from that of MoTiO3. It may be due to the surface coating of MoTiO3 on the GO surface. Fig. 5 illustrates the XRD pattern of prepared samples. As can be seen, the (0 0 1) crystal plane of GO was visible at 10.1. For the $MoTiO_3$ sample, all diffraction peaks were readily indexed to the perovskite phase with a tetragonal structure.

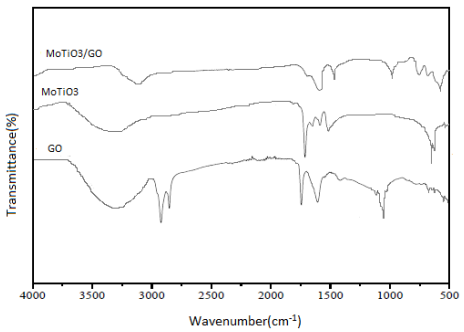

Fig.3. FTIR spectra of GO, $MoTiO_3$ and $MoTiO_3$/ (GO, 1.5 wt. %).

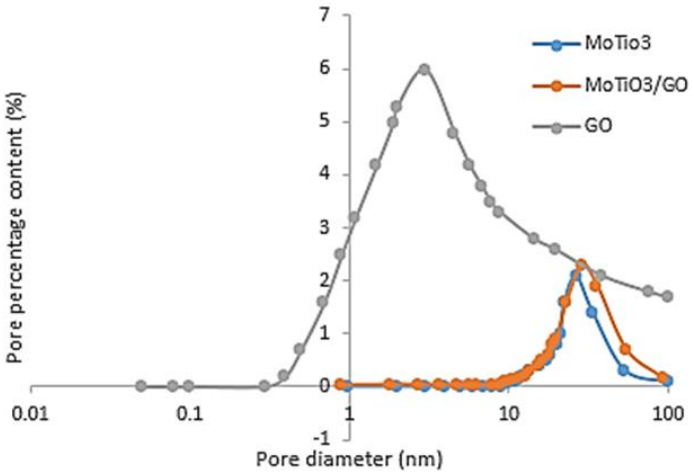

Fig. 4 the average pore size of GO, $MoTiO_3$ and $MoTiO_3$/ GO

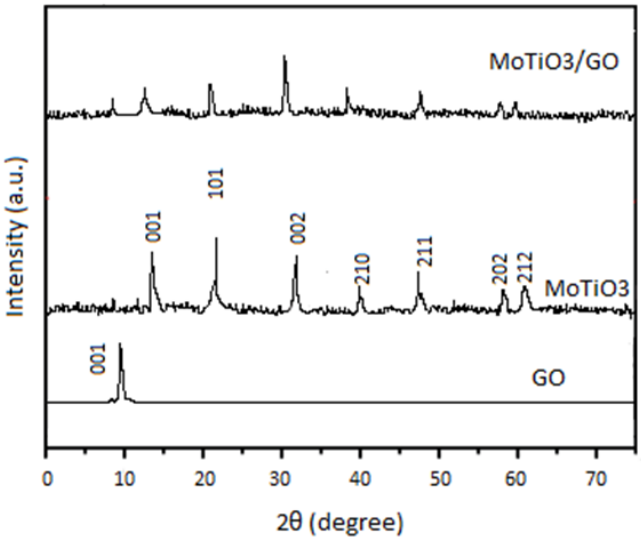

Fig.5 XRD pattern of GO, $MoTiO_3$ and $MoTiO_3$/ (GO, 1.5 wt. %).

The XRD pattern of MoTiO3/GO nanocomposite presented the main diffraction peaks of GO and $MoTiO_3$ and no new diffraction peaks occurred. Compared to the pure MoTiO3 XRD pattern, the intensities of some nanocomposite diffraction peaks decreased due to the placement of MoTiO3 on the GO surface.

For evaluating the adsorption and photo-catalytic degradation, the first step was involved the adsorption of HANs using $MoTiO_3$/GO integrated photo-catalyst adsorbent at dark condition for 60 min. The second step was carried out under UV irradiation (UV-C G20/T8, λ=253 nm) for 2 h. As can be seen in Fig. 6, the absorption amount of HANs on GO is mostly related to the formation of hydrogen bonds between GO hydrogen atoms and HAN nitrogen atoms. MoTiO3/GO showed a much higher absorption efficiency than MoTiO3, which is due to the larger surface area of MoTiO3/GO.

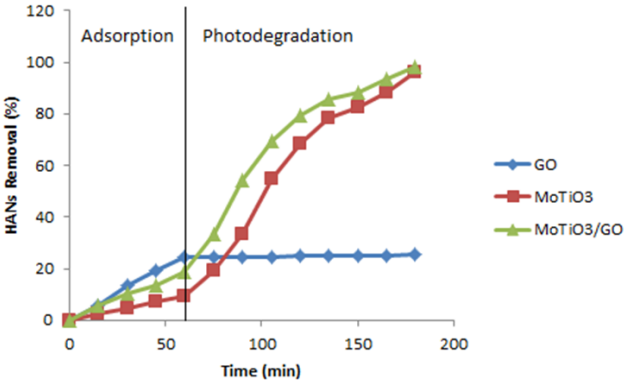

Fig. 6. Adsorption and photo-catalytic degradation of HANs with GO, $MoTiO_3$ and $MoTiO_3$/GO

The data given in Fig. 6 show that the photo-catalytic performance of $MoTiO_3$/GO was higher than that of $MoTiO_3$, which could be related to the specific structure of GO. In fact the hydroxyl groups of GO could generate active hydroxyl radicals by trapping light. The photo-catalytic degradation of HANs was reached to 98.24% after 2 hours of visible light irradiation by MoTiO3/GO, while the photo-degradation by MoTiO3 was reached to 96.13%. The concentration of HANs was decreased only 24.37% by GO, in which adsorption process is dominant phenomenon and UV irradiation has no effect on HANs degradation.

4. Conclusion

The present study showed the application of novel MoTiO3/GO synthetic photo-catalyst adsorbent for the removal of HAN from water. Increasing the content of graphene oxide up to 1.5wt. % in nanocomposite has an increasing effect on specific surface area and consequently the removal of HAN from water. According to SEM result, the spherical particles that placed on the GO surface was observed for MOTiO3/GO nanocomposite. The XRD pattern of MoTiO3/GO presented the main diffraction peaks of GO and $MoTiO_3$ and no new diffraction peaks. Also, the intensities of some diffraction peaks of the MoTiO3/GO decreased due to the coverage of the GO surface by $MoTiO_3$. In the FTIR spectra, some of the stretching vibration band had shifted to lower frequency. Much higher adsorption capacity was observed for $MoTiO_3$/GO than $MoTiO_3$, which was related to the high surface areas of $MoTiO_3$/GO. Also, $MoTiO_3$/GO showed higher photo-degradation performance than others. $MoTiO_3$/ (GO, 1.5 wt. %) successfully eliminate 98.24% of HANs from water for 3 hours.

References

[1] P. Prarat, C. Ngamcharussrivichai, S. Khaodhiar, P. Punyapalakul, J. Hazard. Mater. 192 (2011) 1210.
[2] J. Oyim, E. Amuhaya, R. Matshitse, J. Mack, T. Nyokong, Carbon Trends. 8 (2022) 100191.
[3] G. Yaqub, U. Khan, Z. Sadiq, H. Akram, J. Chil. Chem. Soc. 62 (2017) 432.
[4] M. J. Plewa, E. D. Wagner, M. G. Muellner, K. M. Hsu, S. D. Richardson, 3 (2008) 36.
[5] V. Uyak, I. Koyuncu, I. Oktem, M. Cakmakci, I. Toroz, J. Hazard. Mater. 152 (2008) 789.
[6] P. Prarat, C. Ngamcharussrivichai, S. Khaodhiar, P. Punyapalakul, J. Environ. Sci. 79 (2019) 346.
[7] K. G. Babi, K. M. Koumenides, A. D. Nikolaou, C. A. Makri, F. K. Tzoumerkas, T. D. Lekkas, Desalination, 210 (2007) 215.
[8] J. Kim, B. Kang, Water Res. 42 (2008) 145.
[9] C. Ratasuk, C. Kositanont, C. Ratanatamskul, Sci. Asia. 34 (2008) 293.
[10] X. Chang, X. Yao, N. Ding, X. Yin, Q. Zheng, S. Lu, D. Shuai, Y. Sun, Sci. Total. Environ. 682 (2019) 200.
[11] N. Yahyaa, F. Aziza, N. A. Jamaludina, M. A. Mutalib, A. F. Ismail, W. N. W. Salleha, J. Jaafar, N. Yusof, N. A. Ludin, J. Environ. Chem. Eng. 6 (2018) 7411.
[12] A. M. Alansi, M. Al-Qunaibit, I. O. Alade, T. F. Qahtan, T. A. Saleh, J. Mol. Liq. 253 (2018) 297.
[13] T. A. Saleh, V. K. Gupta, J. Coll. Interf. Sci. 371 (2012) 101.
[14] T. A. Saleh, V. K. Gupta, J. Coll. Interf. Sci. 362 (2011) 337.
[15] K. Peng, L. Fu, H. Yang, J. Ouyang, Scient. Rep. 6 (2016) 19723.
[16] D. Keane, S. Basha, K. Nolan, A. Morrissey, M. Oelgemöller, J. M. Tobin, Catal. Let. 141 (2011) 300.
[17] F. Li, X. Jiang, J. Zhao, S. Zhang, Nano Energy. 16 (2015) 488.
[18] Y. Zhan, J. Lin, Z. Zhu, J. Hazard. Mater. 186 (2011) 1972.